Dominika KOPALA[1], 2. Roman SZEWCZYK[1], 3. Anna OSTASZEWSKA-LIŻEWSKA[1]

Warsaw University of Technology, Institute of Metrology and Biomedical Engineering (1)
ORCID: 1. 0000-0003-4936-0616; 2. 0000-0002-1214-1009, 3. 0000-0002-5203-8129

doi:10.15199/48.2024.10.27

Improved accuracy of FEM fluxgate models based on adaptive meshing

***Abstract**. FEM modelling tools enable testing the sensors' properties under different conditions before they are actually produced. The paper proposed a method of adaptive meshing, which is adjusted to the specific case of fluxgate magnetic field sensors. In this algorithm, the mesh is densified in such a way that skin effect, caused by eddy currents present in those sensors, can be accurately modelled with the use of FEM tools. The paper presents an example of implementation for the fluxgate sensor of Vacquier configuration.*

***Streszczenie.** Narzędzia do modelowania MES umożliwiają testowanie właściwości czujników w różnych warunkach zanim zostaną one wyprodukowane. W artykule zaproponowano metodę adaptacyjnego tworzenia siatki, która jest dostosowana do konkretnego przypadku transduktorowych czujników pola magnetycznego. W tym algorytmie siatka jest zagęszczana w taki sposób, by można było dokładnie zamodelować w narzędziach MES efekt naskórkowości, powstały pod wpływem prądów wirowych występujących w tych czujnikach. W artykule przedstawiono przykład implementacji dla czujnika transduktorowego w układzie Vacquier'a. (**Poprawiona dokładność modeli FEM fluxgate opartych na adaptacyjnym siatkowaniu**)*

Keywords: FEM modelling, adaptive meshes, fluxgate sensors, skin effect
Słowa kluczowe: modelowanie MES, siatki adaptacyjne, czujniki transduktorowe, efekt naskórkowości

Introduction

Magnetic field measurement tools are of great use for their broad application purposes. They play an important role in numerous areas, such as environmental magnetism [1,2] based mainly on rock magnetism [3], archaeomagnetic dating [4], nondestructive testing [5,6] as well as space research [7]. A lot of magnetic sensor types advanced radically in recent years [8,9]. Among them, Fluxgate magnetometers [10] have brought a major interest due to their characteristics [11]. They guarantee high resolution and robustness [12]. Moreover, they are capable of measuring very weak magnetic fields, both AC and DC, which makes them great solutions for measurements in the areas like electronic compasses [13] or bio-medical diagnostics [14]. Due to their bulky nature, however, they might not be suitable for some industrial applications. It made the producers work on planar sensors, which enlarged their capabilities through miniaturization [15]. There are three main configurations of commonly produced fluxgate sensors: ring-shaped core configuration [16], Foerster configuration [17] and Vacquier configuration [18]. They are used primarily due to their higher precision in comparison to other types like single-rod ones [19].

To create a good quality sensor, many factors affecting the sensor's performance need to be taken into consideration. For fluxgate sensors, many of them are related to the ferromagnetic core itself, like the crossfield effect [20], the influence of heat [21] or stress [22] on permeability characteristics. Additionally, such sensors working under an alternate current are subjected to eddy currents [23]. They circulate inside conductors in the form of closed loops, which produce their own magnetic field. This causes the so-called skin effect, which, in case of cylindrical cores, makes a magnetic field gather near the core's surface rather than spread evenly in the core. When modelling suchan effect with FEM tools used to test sensor models, one has to perform more accurate calculations near the core's surface. To do that, a model's mesh needs to be refined in this area since mesh density is related to FEM calculations' accuracy [24]. The method used to perform such a task is adaptive meshing [25].

The paper proposes a specific method of adaptive meshing regarding the influence of skin effect on fluxgate sensors' performance. The adaptive meshing algorithm is implemented with the use of an open-source NETGER mesher [26]. An example is provided with a fluxgate sensor with two rod-shaped cores in the Vacquier configuration. The use of open-source tools enables full access to the source code, which is very useful for educational and implementation purposes. In contrary to other commercial software, such as Ansys [27], the meshing algorithm can be further developed and extended to other modelling cases apart from predefined ones.

Adaptive meshing principles

Adaptive meshing methods base on Delaunay meshing algorithm [28]. It starts with Delaunay triangulation, which divides a given space into triangles. It is done in such a way that the circumcenters of Delaunay triangles are the same as the vertices of the Voronoi diagram [29] built on the same space, as presented in Fig. 1.

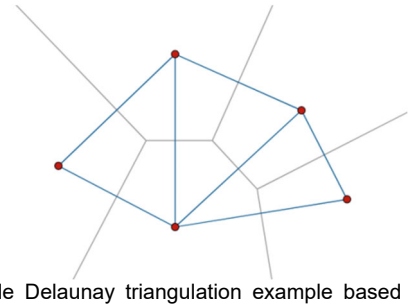

Fig. 1 Simple Delaunay triangulation example based on Voronoi diagram

In the case of 3D objects, the space is divided into tetrahedrons. In such an algorithm, the curvature of an object's edge is the main factor affecting mesh density. This condition makes it difficult to create uniform meshes for cuboid objects, whereas for cylindrical ones created mesh is regular. This dependency is evident in cases where cuboid objects have cylindrically shaped indent, as presented in Fig. 2.

For cylindrical objects, due to their constant radius, regardless of the direction, higher or lower mesh density does not affect its regularity. High-density results in more accurate FEM calculations, but also in more time and computing resources consumption. To avoid this high cost, mesh can be refined only in the area of our interest,

depending on the modelled phenomenon. For this particular case, mesh should be refined in the area near the fluxgate core's surface due to the skin effect.

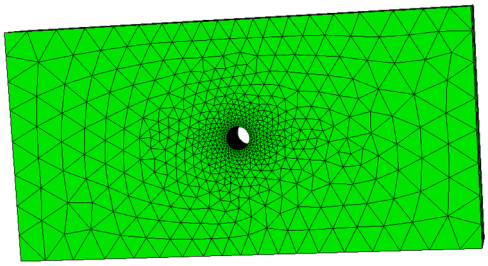

Fig. 2 The example of refining tetrahedral mesh according to the Delaunay algorithm

Adaptive meshing algorithm for fluxgate sensors

Fluxgate sensors, as mentioned previously, can come in different configurations. In this particular case, the Vacquier configuration will be investigated. It consists of two ferromagnetic cores on which two excitation coils are wound. The detection coil is wound around both of cores, which is shown in Fig. 3. Excitation coils are driven by the same current's amplitude but with different directions. It means that if there is no external magnetic field, the detection coil does not receive any signal since signals from both excitation coils sum up to zero. When an external magnetic field occurs, there is an imbalance between the signals produced by both excitation coils, which is detected by the detection coil.

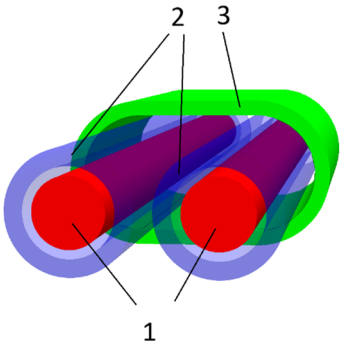

Fig. 3 Fluxgate sensor in Vacquier configuration: 1 - ferromagnetic cores, 2 - excitation coils, 3 - detection coil

Since those fluxgate sensors work under AC current, their case requires in-depth analysis of eddy currents occurring in their cores. Described as the eddy current density $J(r)$, it can be described by the following equations [30]:

$$J(r) = \frac{k \cdot l \cdot J_0(k \cdot r)}{2\pi \cdot R \cdot J_1(k \cdot r)} \tag{1}$$

$$k = \sqrt{\frac{-2\pi f \mu_r \mu_0 j}{\rho}} \tag{2}$$

where I is the driving current, f is its frequency, μ_r is the relative magnetic permeability of the material, μ_0 is the magnetic permeability of vacuum, ρ is the resistivity of the material.

In the above equations, $J_0(x)$ and $J_1(x)$ are Bessel functions of the first kind, of 0 and 1st order, respectively:

$$J_0(r) = \frac{1}{2\pi}\int_{-\pi}^{\pi} e^{-i \cdot x \cdot \sin(t)} dt \tag{3}$$

$$J_1(r) = \frac{1}{2\pi}\int_{-\pi}^{\pi} e^{i \cdot (t - x \cdot \sin(t))} dt \tag{4}$$

According to the form of Bessel functions (3) and (4), the equation (1) is in complex form. Therefore, the amplitude of $|J(r)|$ can be derived as:

$$|J(r)| = \sqrt{\left(reJ(r)\right)^2 + \left(imJ(r)\right)^2} \tag{5}$$

To adjust mesh density to eddy currents, the dependency based on the distance from the core's axis should be derived [31]. Fig. 4 presents the dependency of the amplitude of eddy current density $|J(r)|$ on the distance from the core's axis for different values of driving frequency, where the core's diameter is D = 2 mm and is made of iron with resistivity ρ = 1·10^{-7} Ωm and relative magnetic permeability μ_r = 7000.

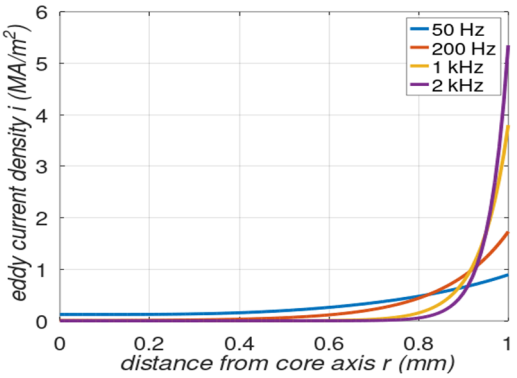

Fig. 4 Eddy currents density across the core's axis for driving frequency f = 50 Hz, 200 Hz, 1 kHz, 2 kHz, core's magnetic permeability μ_r = 7000 and resistivity of the core ρ = 1·10^{-7} Ωm

As it is clearly visible in Fig. 4, the eddy current's amplitude grows at the core's surface and with the growth of the driving current. We can conclude that, especially for higher driving frequencies; mesh needs to be even more refined to analyze skin effect in an accurate way.

The function used to refine the mesh in the adaptive meshing algorithm will be based on equations (1-4). It will modify the size of specific mesh elements near the core's surface. In NETGEN software, this can be controlled by the *maxH* parameter. It defines the maximum height of tetrahedral element. It can be either provided for a whole bulk element or modified locally, which will be used in adaptive meshing algorithm. The modification is done with an additional *msz* file, which provides coordinates of specific lines or points where the mesh should be refined. To avoid manual adjustments for *msz* file, its generation will be done by a script written in an open-source Octave software [32].

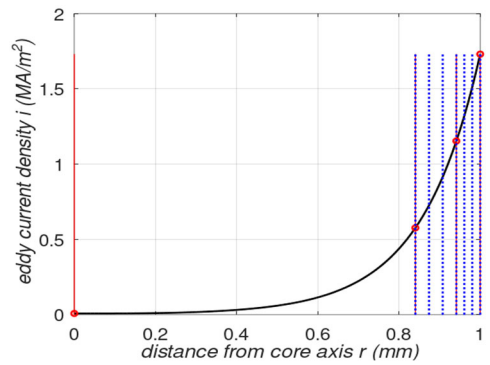

Fig. 5 The principles of layers division for adaptive meshing algorithm, a simulation done for driving frequency f = 200 Hz, core's magnetic permeability μ_r = 7000 and resistivity of the core ρ = 1·10^{-7} Ωm

To calculate a particular *maxH* for a specific area, first the algorithm divides the space between core's axis and its surface (along its radius) by *n1* points, which creates *n1 -1* areas. Next, each section is divided into *n2* layers. The maximum height of a tetrahedral element in a selected area will be equal to the distance between specific layers. The number of divisions *n1* and *n2* are selected by the user. Thanks to such a choice, the user has full control over the required mesh quality so that the user can make density lower or higher to his own choice. The division method is presented in Fig. 5.

The software is designed to refine the mesh of two-core fluxgate sensors, so the user also needs to define geometric parameters of the model, such as the cores' axes' coordinates and cores' radii. Fig. 6 presents a preview of the points where mesh will be refined on the plane of the cores' cross-sections.

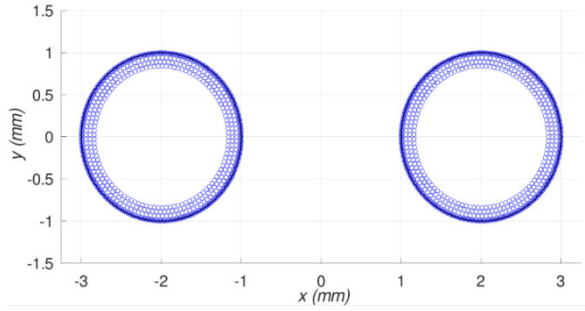

Fig. 6 Preview of the points where mesh is refined, the example for Vacquier fluxgate sensor with two cores, R = 1 mm

After generating a set of points, just like in Fig. 6, a mesh file *msz* is generated. It refines mesh on the lines crossing given points and in parallel to the cores' axes. However, *msz* file is not sufficient to generate the full Vacquier model's mesh since *msz* file describes only the places of refinement. The geometric model written in NETGEN software using *geo* file, which includes geometry description (like object coordinates), can additionally include basic information on mesh size for each element.

To combine mesh information from geo and *msz* file, the *msz* file needs to be attached to the geometric model before the meshing process begins. As a result, NETGEN generates the final mesh with the required quality. It is important to note that the basic mesh *maxH* parameter needs to be higher than *maxH* calculated by the refined mesh algorithm. Otherwise, the results of refinement by *msz* file may not be visible. The comparison between basic and refined mesh is presented in Fig. 7 and Fig. 8.

The example is provided for Vacquier fluxgate sensors with iron cores for driving frequency f = 200 Hz. The area near the core's surface was divided into seven subareas (n_1 = 3, n_2 = 3), within which mesh was densified. As it can be seen, the algorithm made basic NETGEN mesh more dense around the surface of both cores, where the amplitude of eddy currents is the highest, whereas near the core's axis, the mesh remains coarse.

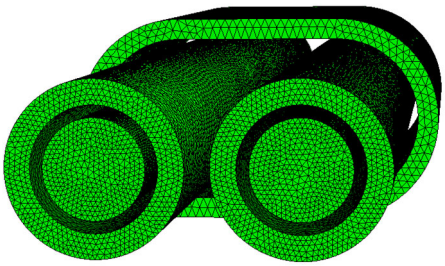

Fig.7 Basic NETGEN generated mesh - not refined by *msz* file

In this particular example, standard mesh with no refinement has around 1.3 million elements (the exact number is 1 345 444), where the lowest *maxH* parameter is 0.2 mm for both cores. Mesh with *msz* file refinement has got the lowest *maxH* of approximately 0.02 mm near the core's surface and consists of approximately 70 million elements (the exact number is 70 050 588). If we wished to have maxH this low for both cores' volumes, the mesh would consist of about 12.5 million elements (the exact number is 12 543 796). Regarding elements number, the solution would suggest fewer elements for locally refined mesh than for fully refined. However, the parameter that counts in FEM models is the number of nodes in the mesh for which solutions are calculated. When comparing them for a single core only, for basic mesh, the model consists of around 53 thousand nodes (the exact number is 52 675). The locally refined core mesh consists of approximately 9 million nodes (the exact number is 8 754 496), whereas the fully refined one consists of approximately 14 million nodes (the exact number is 14 360 854), which is almost 1.5 times more than for the local refinement. In comparison to fully refined mesh with the same *maxH* in its whole volume, the presented solution results in much fewer nodes for which the solutions are calculated. In a result it will make FEM model much less time and computational cost-consuming.

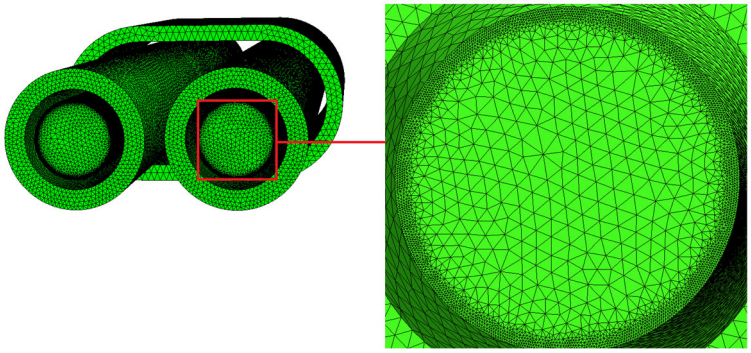

Fig.8 NETGEN mesh refined by *msz* file

Conclusions

During the analysis of FEM fluxgate sensor models, eddy currents causing skin effect in rod-shaped cores need to be taken into account. Simple meshes with a basic Delaunay algorithm may not be sufficient to analyze surface-focused phenomena.

The paper proposes a sufficient algorithm of local mesh refinement for two rod-shaped cores fluxgate sensors. Based on the Vacquier type test case, it refined mesh near the core's surface according to the local amplitude of eddy currents. The algorithm connects eddy currents' amplitude with the maximum height of tetrahedral mesh element

maxH. As a result, the generated mesh is suitable for FEM analysis of eddy currents and skin effect occurring in such fluxgate sensors. Moreover, using open-source tools like NETGEN or Octave software enables easy development and usage of the proposed algorithm in other test cases.

Acknowledgments: *The research was co-founded by Warsaw University of Technology within the Excellence Initiative: Research University (IDUB) programme.*

Supplementary materials

The source code of the algorithm can be downloaded at: https://github.com/DKopala/FluxgateAdaptiveMesh.

Authors*: mgr inż. Dominika Kopala, Politechnika Warszawska, Instytut Metrologii i Inżynierii Biomedycznej, ul. św. Andrzeja Boboli 8, 02-525 Warszawa, E-mail: dominika.kopala.dokt@pw.edu.pl; prof. dr hab. inż. Roman Szewczyk, Politechnika Warszawska, Instytut Metrologii i Inżynierii Biomedycznej, ul. św. Andrzeja Boboli 8, 02-525 Warszawa, E-mail: roman.szewczyk@pw.edu.pl; dr inż. Anna Ostaszewska-Liżewska, Politechnika Warszawska, Instytut Metrologii i Inżynierii Biomedycznej, ul. św. Andrzeja Boboli 8, 02-525 Warszawa, E-mail: anna.lizewska@pw.edu.pl.*

REFERENCES

[1] Liu Q., Roberts A. P., Larrasoaña J. C., Banerjee S. K., Guyodo Y., Tauxe L., Oldfield F., Environmental magnetism: Principles and applications, *Reviews of Geophysics*, Vol. 50, Issue 4, 2012, RG4002. DOI: 10.1029/2012RG000393

[2] Thompson R., Bloemendal J., Dearing J. A., Oldfield F., Rummery T. A., Stober J. C., Turner G. M., Environmental Applications of Magnetic Measurements, *Science*, Vol. 207, No. 4430, 1980, pp. 481-486. DOI: 10.1126/science.207.4430.481

[3] Dunlop D. J., Özdemir, Ö., Rock Magnetism: Fundamentals and Frontiers, *Cambridge University Press,* 1997, DOI: 10.1017/CBO9780511612794

[4] Brock A., Magnetic Dating Methods in Prehistory, *The South African Archeological Bulletin*, Vol. 32, No. 125, 1977, pp. 5-13. DOI: 10.2307/3887842

[5] Hu B., Yu R., Zou H., Magnetic non-destructive testing method for thin-plate aluminium alloys, *NDT & E International*, Vol. 47, 2012, pp. 66-69. DOI: 10.1016/j.ndteint.2011.12.007

[6] Cardelli E., Faba A., Marsili R., Rossi G., Tomassini R., Magnetic nondestructive testing of robot blade tips, *Journal of Applied Physics*, Vol. 117, No. 17, 2015, pp. 17A705. DOI: 10.1063/1.4907180

[7] Jannet, G., Dudok de Wit, T., Krasnoselskikh, V., Kretzschmar, M., Fergeau, P., Bergerard-Timofeeva, M., et al., Measurement of magnetic field fluctuations in the Parker Solar Probe and Solar Orbiter missions, *Journal of Geophysical Research: Space Physics*, Vol. 126, No. 2, 2021, pp. e2020JA028543. DOI: 10.1029/2020JA028543

[8] Gazda P., Szewczyk R., Novel Giant Magnetoimpedance Magnetic Field Sensor, *Sensors*, Vol. 20, No. 3, 2020. DOI: 0.3390/s20030691

[9] Morten B., De Cicco G., Prudenziati M., Masoero A., Mihai G., Magnetoresistive thick film sensor for linear displacements, *Sensors and Actuators A: Physical*, Vol. 46, No. 1, 1995, pp. 261-265. DOI: 10.1016/0924-4247(94)00902-T

[10] Ripka P., Review of fluxgate sensors, *Sensors and Actuators A: Physical*, Vol. 33, Issue 3, 1992, pp. 129-141. DOI: 10.1016/0924-4247(92)80159-Z

[11] Kaluza, F., Grüger, A., Grüger, H., New and future applications of fluxgate sensors, *Sens. Actuators A Phys.*, Vol. 106, 2003, pp. 48–51. DOI: 10.1016/S0924-4247(03)00131-6

[12] Primdahl F., The fluxgate magnetometer, *J. Phys. E Sci. Instrum*, Vol. 12, 1979, pp. 241-253. DOI: 10.1088/0022-3735/12/4/001

[13] Baschirotto, A., Dallago, E., Malcovati, P., Marchesi, M., Venchi, G. Precise vector-2D magnetic field sensor system for electronic compass. *SENSORS, 2004 IEEE*, Vienna, Austria, 24–27 October 2004, Vol. 2, pp. 1028–1031. DOI: 10.1109/ICSENS.2004.1426349

[14] Tomek, J., Platil, A., Ripka, P., Kašpar, P., Application of fluxgate gradiometer in magnetopneumography. *Sens. Actuators A Phys.*, Vol. 132, 2006, pp. 214–217. DOI: 10.1016/j.sna.2006.02.033

[15] Neosha N., Roshanghias A., Lenzhofer M., and Ortner M., Analysis of Single- and Double Core Planar Fluxgate Structures, *Proceedings*, Vol. 2, No. 13, 2018, pp. 831. DOI: 10.3390/proceedings2130831

[16] Primdahl, F., Brauer, P., Merayo, J.M.G., Nielsen, O.V., The fluxgate ring-core internal field, *Meas. Sci. Technol.*, Vol. 13, No. 8, 2002, pp. 1248. DOI: 10.1088/0957-0233/13/8/312

[17] Gaffney, C., Gaffney, V., Cuttler, R., Yorston, R., Initial results using GPS navigation with the Foerster magnetometer system at the World Heritage site of Cyrene, Libya. *Archaeol. Prospect.*, Vol. 15, 2008, pp. 151-156. DOI: 10.1002/arp.330

[18] Gavazzi B., Le Maire P., de Lepinay J. M., Calou P., Munschy M., Fluxgate three-component magnetometers for cost-effective ground UAv and airborne magnetic surveys for industrial and academic geoscience applications and comparison with current industrial standards through case studies, *Geomechanics for Energy and the Environment*, Vol. 20, 2019, pp. 100117. DOI: 10.1016/j.gete.2019.03.002

[19] Ripka P., Advances in fluxgate sensors, *Sensors and Actuators A*, Vol. 106, 2003, pp. 8-14. DOI: 10.1016/S0924-4247(03)00094-3

[20] Ripka P., Janosek M., Butta M., Billingsley S. W., Wakefield E., Crossfield effect in magnetic sensors, *Sensors, 2009 IEEE*, pp. 1860-1963. DOI: 10.1109/ICSENS.2009.5398405

[21] Mandava S., and Ramachandrula S., Yarramareddy A., Effect of Thermal Treatment of a Ferro Magnetic Core on Induced EMF, *Procedia Materials Science*, Vol. 6, 2014, pp. 436-443. DOI: 10.1016/j.mspro.2014.07.056

[22] Birss R.R., Faunce C.A., Isaac E.D., Magnetomechanical effects in iron and iron-carbon alloys, *Journal of Physics D: Applied Physics*, Vol. 4, No. 7, 1971, pp. 1040-1048. DOI: 10.1088/0022-3727/4/7/322

[23] Kriezis E.E., Tsiboukis T.D., Panas S.M., Tegopoulos, J.A., Eddy currents: theory and applications, *Proceedings of the IEEE*, Vol. 80, No. 10, 1992, pp. 1559-1589. DOI: 10.1109/5.168666

[24] Pisarciuc C., Dan I., Cioară, R., The Influence of Mesh Density on the Results Obtained by Finite Element Analysis of Complex Bodies, *Materials*, Vol. 16, No. 7, 2023, pp. 2555. DOI: 10.3390/ma16072555

[25] Lindgren L. E., 7 - Numerical methods and modelling for efficient simulations, Computational Welding Mechanics, *Woodhead Publishing*, 2007, pp. 80-98. DOI: 10.1533/9781845693558.80

[26] Netgen/NGSolve: https://ngsolve.org/ (accessed May 30, 2023)

[27] Ansys Blog: How to Accelerate Ansys Fluent Simulations with Adaptive Meshing: https://www.ansys.com/blog/how-to-accelerate-ansys-fluent-simulations-with-adaptive-meshing (accessed May 30, 2023)

[28] Cheng SW., Poon SH., Three-Dimensional Delaunay Mesh Generation, *Discrete Comput. Geom.*, Vol. 36, Issue 3, 2006, pp. 419-456. DOI: 10.1007/s00454-006-1252-5

[29] Aurenhammer F., Voronoi Diagrams – a Survey of a Fundamental Geometric Data Structure, *ACM Comput. Surv.*, Vol. 23, No. 3, 1991, pp. 345-405. DOI: 10.1145/116873.116880

[30] Temme N. M., Special Functions: An Introduction to the Classical Functions of Mathematical Physics, *John Wiley & Sons, Inc.*, New York, 1996

[31] Ostaszewska-Liżewska A., Kopala D., Szewczyk R., Improved Control of Mesh Density in Adaptive Tetrahedral Meshes for Finite Element Modeling, *Pomiary Automatyka Robotyka*, Vol. 26, No. 2, 2022, pp. 23-28. DOI: 10.14313/PAR_244/23

[32] GNU Octave: https://octave.org (accessed May 30, 2023)